IEEE Transactions on Geoscience and Remote Sensing
July 2012 ; Volume 50 (7) : Pages 2639 - 2648
http://dx.doi.org/10.1109/TGRS.2012.2184124
© 2012 IEEE

Archimer
http://archimer.ifremer.fr

Enhanced Arctic Sea Ice Drift Estimation Merging Radiometer and Scatterometer Data

Fanny GIRARD-ARDHUIN* and Robert EZRATY

IFREMER, Laboratoire d'Océanographie Spatiale, BP 70, 29280 Plouzané, France

*: Corresponding author : F. Girard-Ardhuin, email address : fanny.ardhuin@ifremer.fr

Abstract:

Satellites enable daily and global coverage of the polar oceans and provide a unique monitoring capability of sea ice dynamics. Sea ice drift maps can be estimated in Arctic from several satellite sensors, particularly from scatterometers and radiometers. This study presents the benefits of combining single drift fields at the same resolution into a "merged" field, built at three- and six-day lags during winters with a 62.5-km resolution. It is shown that combining these drift fields not only increases the reliability of the displacement estimation and the number of estimated vectors to almost a full ice covered area but also expands the time period over which these estimations are reliable from freeze until the melt onset. The autumn-winter-spring sea ice drift fields presented here are systematically produced at Institut Français de Recherche pour l'Exploitation de la Mer/Centre d'Exploitation et de Recherche Satellitaire, the sea ice drift 1992-2011 time series is available, and the processing is ongoing. These data are available for operational use and for the scientific community.

I. Introduction

Sea ice cover and motion have major effects on heat fluxes between ocean and atmosphere. Moreover, the Arctic ice growth and melt impact the fresh water flux which plays an important role in the thermohaline circulation [1]. The Arctic sea ice motion features depend on atmospheric (wind) and oceanic forcings (surface currents). The mean short term motions are well known [2], they follow mainly the synoptic weather systems. For long-term estimation, oceanic currents should be considered. The main features are the transpolar drift from the Siberian coast across the North Pole towards the Fram Strait, and the anticyclonic motion in the Beaufort Sea. Nevertheless, at shorter time-scale, the motion is highly variable. Therefore, sea ice motion observations are required for day to day monitoring.

The sea ice motion measurements have started with ships observations (the Nansen's expedition in 1893-96) and some manned drifting stations. Since 1979, about twenty buoys per year are moored on Arctic ice in the frame of the International Arctic Buoy Programme (IABP). They provide continuous local measurements, covering mostly the Central Arctic and Beaufort Sea, but the spatial distribution is rather sparse in the Eurasian Seas, providing a limited view of the velocity field [2]. Since the 1990's, sea ice drift can be estimated from satellite data, with daily and global coverage of the polar oceans. In order to determine an ice cover displacement, surface patterns compatible in size with the sensor spatial resolution and satellite repeat cycle must persist for several days. A major difference between satellite and buoys measurements is that buoys are representative of single points displacement while satellite sensor provides information over the foot-print area. For limited time duration, demonstration, and/or local or regional studies, high spatial resolution satellite sensors have

been used to estimate sea ice drift, for example with Advanced Very High Resolution Radiometer (AVHRR) data [3], Seawinds/QuikSCAT enhanced resolution data [4] and Synthetic Aperture Radar (SAR) data [5-6 among others].

The basic information needed for drift estimation are daily maps of physical properties which have to remain stable for a short period, typically two to six days. At low resolution, the brightness temperature data from Special Sensor Microwave Imager (SSM/I) radiometers onboard Defense Meteorological Satellite Program have been widely used, and also the backscatter data from SeaWinds/QuikSCAT scatterometer.

Several methods exist to infer sea ice drift from single sensors and it is not the purpose of this paper to discuss them. This paper deals with techniques applied to these single drift sensors to combine them to a "merged" product with several benefits, in particular high data density and an expanded time period of estimation, including freeze period. Section II briefly describes our method to infer drift estimation from single sensors like radiometer and scatterometer. Section III is the focus of the paper describing the combination of these single drift vectors fields to a merged product, the validation results of this product against IABP buoys data are shown. The advantages and shortcomings of these measurements are presented in the Section IV.

II. Single sensor sea ice drift estimation

Sea ice drift fields at global scale exist since the beginning of the Arctic monitoring with the low frequency channels of the SSM/I radiometer sensor. Sea ice drifts deduced from

radiometers have a reasonable accuracy but are limited by data gaps inducing low data density at the beginning and the end of the cold period due to rapid changes in the estimated brightness temperatures. This can be improved using scatterometer data to built a merged field.

The single sensor drift estimation is presented in Section II.B after a quick description of the sensors used in Section II.A.

A. Sensors

We present here the sensors we use in the following drift estimation and merging process : SSM/I and Advanced Microwave Scanning Radiometer – Earth Observing System (AMSR-E) radiometers and QuikSCAT and Advanced Scatterometer (ASCAT) scatterometers.

Data of passive microwave radiometers onboard satellites such as SSM/I have been commonly used to estimate sea ice concentration from the daily brightness temperature maps. Data have also be used for sea ice drift estimation with good accuracy (Table 1). The pixel resolution is 25 km when using the lower frequencies at 19, 22 and 37 GHz, we use here the 85.5 GHz channel data (at Horizontal –H- and Vertical –V- polarizations) with the higher pixel resolution of 12.5 km that is available since 1992.

AMSR-E is a passive microwave radiometer sensor with several channels and several frequencies ranging from 6.9 to 89.0 GHz and both H and V polarizations. Compared to the high frequency resolution of the SSM/I 85 GHz channels, the 89 GHz channels of AMSR-E resolution is better, enabling mapping the 89 GHz brightness temperature maps with a pixel

size of 6.25 km x 6.25 km. These data are available since 2002, they are used here for a medium resolution merged drift product.

These two radiometers have a wide data gap at the North Pole. Thanks to different satellite orbit configurations and instrument setups, the two scatterometers presented here enable to have a reduced data gap at North Pole. The Ku-band SeaWinds/QuikSCAT scatterometer provides two backscatter fields from the inner and outer beam (respectively at H and V polarizations at 46° and 54° incidence angles). Daily averaged backscatter maps at the resolution of 12.5 km have been built from these data from 1999 until 2009 (end of QuikSCAT) and used for sea ice drift estimation.

The European C-band vertically polarized ASCAT onboard MetOp can be used since 2007, it is composed of three fan-beam antennas pointing to the left-hand side of satellite track and the same arrangement on the right-hand side, with incidence angles ranging from 25° to 65°. Backscatter values over sea ice are function of both the incidence angle and the sea ice type [7] and one advantage of QuikSCAT data is that they do not require incidence angle adjustment like ASCAT data. With ASCAT several incidences measurements, an incidence adjustment is mandatory over sea ice to map daily averaged backscatter values accurately for geophysical use. Backscatter data can only be mapped conveniently if a model is used to compensate for this effect. An incidence-adjustment backscatter map at 40° incidence angle is thus built in order to have reliable daily averaged backscatter maps. These daily backscatter ASCAT maps are available at Institut Français de Recherche pour l'Exploitation de la MER (IFREMER)/Centre d'Exploitation et de Recherche SATellitaire (CERSAT).

We can note here that ASCAT C-band scatterometer provides more data over the Arctic area than the previous C-band sensor Active Microwave Instrument (AMI) onboard European

Remote Sensing (ERS) satellite, first because of the six beams instead of three, and second because the SAR onboard ERS can not operate simultaneously with the scatterometer (missing data). These improvements enable to build daily backscatter maps at 12.5 km resolution, which was not possible in the 1990's with AMI (weekly maps at 25 km grid size).

All these data are used to infer single sensors sea drift fields (see Section II.B) from which a merged product is processed (Section III).

B. Method

The focus of the paper is the merging of drift fields, for that we need first to present the single sensor drift fields.

Passive microwave radiometers data like SSM/I brightness temperature data have been widely used to estimate Arctic sea ice drift. Low resolution passive microwave data are very sensitive to atmospheric effects (moisture and liquid water) and snow and ice properties [8]. In order to determine sea ice drift from successive brightness temperature maps, stable radiation of the sea ice cover and negligible influence of the atmospheric conditions are required. This implies sea ice drift estimations are only possible during winter, from October until April [9]. The benefit of the all-weather, day-night microwave radar measurements has been well established. Radars at Ku-band do not have the problem caused by water vapour as the 85.5 GHz SSM/I channels, which makes QuikSCAT an adequate sensor to fill in the poorly monitored areas where the weather influence prevents reliable SSM/I estimation during the cold season [10]. The microwave response of sea ice is greatly influenced by the changes of properties of sea ice which becomes a wet surface during summer [11]. During warm months,

sea ice properties change quickly, so that surface, atmosphere, and brightness temperature measurements are unstable, drift estimation is thus practically impossible during this period.

Tracking methods assume that the structures tracked have spatial dimensions larger than the pixel resolution. Several methods exist to determine sea ice displacements, algorithms are based on tracking common features on pairs of sequential satellite maps. The method applied here is the most widely used : the Maximum Cross Correlation (MCC) between successive and lagged maps [9, 12, 8, 4], it was successfully used first with AVHRR data [3, 13]. This only enables detection of translation displacement and no rotation [13-14]. A correlation is estimated between two arrays (blocks) of data : one at a given day and another one lagged in time, the location of the maximum correlation is the location of the maximum similarity between the two original sub-images. The displacement can thus be inferred, details of the MCC tracking method can be found among others in [12, 8, 9]. A displacement of less than half a pixel size is estimated as no-displacement, this is a known problem of MCC tracking method [8], directly linked with the pixel size. A refinement called Continuous MCC (CMCC) is based on MCC and relies on a continuous optimization step for computing the motion vector, reducing this noise [15]. Here, we use the MCC because it has proven to be robust and simple, and it has been well validated [3, 13, 4, 9].

For the single sensor drift products presented here, the data processing can be split into three main steps :

1) construction of the second derivative fields (Laplacian and smoothing) of daily maps at D Day and D+3 for 3-day lag motion estimation (D+6 for 6-day lag)
2) application of the correlation algorithm between D and D+3 (D and D+6) maps
3) quality control of the displacements

These are the details of these steps through the example of SSM/I processing chain. We start to apply preliminary processing on the D Day, D+3 and D+6 daily brightness temperature maps at 85.5 GHz H and V channels where an open water/sea ice discrimination is performed (the ice boundary corresponds to 15% sea ice concentration, estimated with the Artist Sea Ice algorithm [16]). A single composite map of the H and V channels data is not possible since each channel responds to different physical properties, the two channels maps are processed separately.

First, a Laplacian filter is applied over a 5 x 5 pixels grid in order to enhance the structures to be tracked and to stabilize them in time, filtering out the mean level shifts. This also implies that any value of the resulting field closer than three cells of a land boundary must be discarded, to overcome this problem, land and islands boundaries are extended by three pixels. Wavelet analysis, applied by [17, 10], is very similar to the Laplacian field enhancement technique applied here. Second, median filter is applied over a 3 x 3 pixels array in order to smooth the field. Tests have shown that these preliminary steps increase the displacement estimation ability. The MCC is thus applied on this last field at 12.5 km resolution with a cross-correlation array of 11 x 11 pixels. It can be shown that the quantification noise accounts for $L^2/6$ in variances where L is the pixel size, in our case, this corresponds to 5.1 km. Future plans are to reduce this effect. The spacing between the inferred vectors is 5 pixels which is 62.5 km, adjacent vectors are thus not completely independent because of the overlap between adjacent cross-correlation arrays (neighboring arrays share half their pixels).

To remove outliers, a minimum correlation coefficient threshold of 0.60 is imposed (0.30 for [8, 15]). Then, a quality control of the likely ice motion vectors is performed with two steps. First, for short time scale, mean sea ice drift is strongly driven by the winds in dynamical

areas [18], and a control of the sea ice drift direction with wind direction of the European Center for Medium-range Weather Forecasts model is applied ([8] did the same with the National Centers for Environmental Prediction re-analyses), the drift estimation is valid where the angular difference between satellite estimation and wind is less than 80° (60° for [8]). Second, the spatial consistency of the motion fields is controlled on a 24 x 24 pixels area (312.5 km x 312.5 km). It is based on the comparison of the local motion vector and the surrounding vectors.

The lag time that we can use to estimate the vector displacement has been tested : in the Arctic, drift maps can be computed for two to three-day lag, while around Antarctica, less than one-day lag should be used. Note that with a pixel resolution of 12.5 km, for one-day lag, the minimum displacement that can be measured using the MCC is 6.25 km which corresponds to a velocity of 7 cm s^{-1}, the mean sea ice velocity is of the same order (estimated from buoys data from five winters). Then the lags to be used must be higher: three-day lag corresponds to a minimum velocity of 4.8 cm s^{-1} , it is commonly used [9 among others]. But, the day lag must be chosen accordingly to the magnitude of the expected drift. It is thus useful to estimate drift at both short and large lags: we process three and six-day lag with the low resolution product (SSM/I, QuikSCAT, ASCAT). A two-day lag is also commonly used [15], we propose drifts at two-day lags also using the AMSR-E medium resolution drift fields.

Sea ice drifts maps are thus inferred from SSM/I-H and SSM/I-V daily maps at three and six-day lags during winter months. The same processes are applied to the backscatter fields of scatterometer data of QuikSCAT and ASCAT at the same grid resolution. Thanks to the sensor geometry and satellite orbits, the data gap area at the North Pole is lower for these sensors than for SSM/I (254 km radius). For the QuikSCAT sensor, H and V channels data

are available at 46° and 54° incidence angle respectively. For Ku-band backscatter data, it was shown that over sea ice and at the same incidence angle, the ratio between V polarization data and H polarization data is almost constant [19]. Thus the backscatter difference between the two QuikSCAT channels can be mainly attributed to the incidence angle difference (which remain constant), it makes it possible to combine the two channels data in a composite backscatter map as the average of the two beams maps. The remaining data gap area (about 30 km radius) is then filled in using quadratic surface interpolation using the surrounding values. This final composite map is used to follow the steps 1 to 3 presented before in order to infer sea ice drift maps from this sensor.

ASCAT data are also used for sea ice drift estimation, with the same grid resolution as SSM/I and QuikSCAT fields. AMSR-E H and V brightness temperature maps are used for sea ice drift estimation enabling a medium-resolution drift field (31.25 km drift grid size).

From these single sensors drift maps, we have built merged drift maps. They present several advantages.

III. Merging the sea ice drift fields

In this section, we will describe the merging of single sensor/channel drift products. The low resolution drift product merging SSM/I 85 GHz H and V channels with QuikSCAT or ASCAT drift data is presented in Section III.A. A medium-resolution product merging AMSR-E H and AMSR-E V channels is presented in Section III.B.

A. Low resolution product

Single sensors sea ice drift maps are built at three and six-day lags from SSM/I-H, SSM/I-V, QuikSCAT and ASCAT at 62.5 km drift grid size. The problem of systematic missing data area at North Pole with SSM/I data can be solved with the use of scatterometer data like QuikSCAT and ASCAT where the gap is small (about 30 km radius). Since the vectors fields are computed with the same pixel resolution, the drift are estimated at the same grid size: the statistical properties are identical and thus the drifts fields can be merged.

We will describe here the "merged" product with the example of SSM/I-H, SSM/I-V and QuikSCAT data. The core of this merging relies on previously validated single sensor drift data. The main steps of the merging are presented here:

1) initialisation phase

2) selection of a drift vector

3) quality control

The analysis of possible combination at a single-grid node indicates fourteen possible cases ranging from a triplet of identical vectors to either three different estimations or even a single available vector. The first step consists in giving weight at each drift grid-nodes. Higher the confidence in the drift data, the less weight is given. The weight depends on the selection/quality control procedure and on the selected sensor or channel. The minimum weight is given to the scatterometer vectors since they are in better agreement with reference data than radiometer vectors (for example [10]). For example, an identical triplet drifts correspond to weight of one, identical pairs to two (if containing scatterometer vector) or

three (SSM/I only) depending on the sensor, single sensor drift to four (scatterometer) or five (SSM/I channel).

The cases where several drifts vectors exist (triplet, pairs) are treated differently from the cases where a single vector only is available. Both procedures use the surrounding and quality controlled vectors of the merged drift field. For the case of triplet or pairs, a selection must be done, based on a cost-function, which is function of both the weight attached to each vector, related to the confidence in the drift data, and the distance between grid-node of the vector tested and the grid-nodes of the surrounding vectors. For the case of single vector, it has to be controlled by comparison to the surroundings drift vectors. The goal of this step is to test the spatial consistency of the drift vectors (in a 5 x 5 pixels grid node geometry) since few number of outlier vectors may remain, mainly at discontinuities or at the edges of the drift grid. A loop is performed until no new vector is added: at the beginning, this step is processed with a background map composed of not-yet accepted vectors from the three drift maps, at the end only the already accepted vectors of the merged map are used as background for this step. A flag is linked to each accepted drift vector, detailing the selection and quality control criteria.

A merged field based on the combination of SSM/I drifts and scatterometer drifts has been built daily during the “cold” season, which is autumn-winter-spring. The product has been computed at three and six-day lags during the QuikSCAT period (1999-2009) and is ongoing and continuous with SSM/I drift fields merged with ASCAT scatterometer drift fields since 2007. The merged drift estimation for 24 until 27 April in 2007 from SSM/I and QuikSCAT is shown in Fig. 1. Colours of the arrows corresponds to the merged processing for each pixel: in red, the three estimation are identical (scatterometer and radiometer H and V estimation), in

green, two of the three drifts are identical, in blue, one channel has been chosen. The sea ice drift patterns are moving from day to day, and Fig. 1 presents a pattern which is representative for a “classical” drift pattern with the Beaufort gyre, a southward drift in Fram Strait, and ice export out of Kara Sea.

Radiometers and scatterometers have been extensively used for sea ice drift estimation, the validation of single sensors drift products with buoys show good accuracy, Table 1 presents some results of validation experiments [8, 10, 12, 17, 20]. The merged drifts are compared with IABP buoys drifts at three and six-day lags. Results are presented in Table 2 through drift magnitude and direction parameters and also with u/v components -East/North- whereas most of the results of previous studies for single sensor drifts (Table 1) are presented in velocity parameter. The velocity has been added in Table 2 for information, due to our method, the constant half-pixel minimum displacement embedded in the original measurement is then erroneously accounted for.

Note that it is very difficult to compare and to conclude from validation results, mainly because of the different buoys datasets, methodologies, areas, time periods, etc... Moreover, the results have been reported with several scales (drift magnitude and direction, East and North components, X and Y axis components, ice velocity). The drift estimation is a mean displacement and not a velocity and usually, the estimated displacements are converted into ice speed in order to compare the quality of the drift magnitude estimated at different day-lags or at various pixel size (Table 1), even though this transformation is non-linear. This problem of the comparison of results has been discussed and highlighted with more details in [15].

Our validation of the merged product is based on data from five winters. At three-day lag, most of the drift magnitude values we estimate are less than 30 km (less than three pixels

displacements), and there is a good agreement between the data. The standard deviation of the difference to buoys is 7.5 km. Drifts data are converted into ice speed in order to compare with previous single sensors results. The standard deviation of the difference of ice speeds from the merged product at three-day lag corresponds to 2.91 cm s^{-1}, which is comparable with previous validation results shown also in Table 1, from 2.6 to 11 cm s^{-1}. Previous studies have compared buoys and satellite drifts with and without small drifts [8, 20]: their results show smaller standard deviation when small drifts magnitudes (lower than one pixel) are dismissed. Excluding small drifts magnitudes for validation is questionable since drifts lower than one pixel can be very common (24% of the merged drifts in this validation), modifying strongly the statistics of the samples.

As expected, angles of drift vectors inferred with the MCC method present a strong uncertainty for small drifts (lower than two pixels in component). At three-day lag, the standard deviation of the angle difference between buoys and our merged satellite product is 39.2°; if drifts less than one pixel are excluded, the standard deviation decreases down to 29.6° thus excluding small drifts improves significantly the angular accuracy. Fig. 2 shows the angle difference between the merged product and buoys as a function of merged drifts magnitudes : the angle difference sharply decreases (smaller than 45°) for drifts magnitudes higher than 40 km (about three pixels), this was also noticed by [10]. This result in drift direction is comparable to previous validation results presented in Table 1, ref. [8] improves also strongly the angle comparison at three-day lag excluding small drifts.

Using six-day lag is more adequate to small drifts measurements. The standard deviation of drifts difference to buoys drift at six-day lag is 8.9 km. With six-day lag, the standard deviation of the velocity difference is lower than with three-day lag as expected (1.72 cm s^{-1} at

six-day lag and 2.91 cm s^{-1} at three-day lag). Six day-lag is better for small drifts magnitude estimation, consequently, the angle data have a better resolution with a standard deviation of the difference of 29.6°, comparable to the results shown in Table 1. Comparing buoys and merged drifts in North/East components frames enables independent estimate of uncertainties and is needed for use in models: the standard deviation of the difference are the same for North and East : 7.0 km at three-day lag and 8.2 km at six-day lag.

The data density is defined as the percentage of vectors available over the sea ice area for a given day. Fig. 3 shows the drift data density at three-day lag from September 2007 until May 2008. Individual sensors drift data densities are shown in green and blue for SSM/I radiometer (at H and V polarization respectively), in black for ASCAT scatterometer, and the merged field data density is in red. Radiometer data (SSM/I) have 40% to 70% data density from October until end of April and a limited number of drift data at the beginning and the end of the winter (from 15 to 40% in September, 20 to 60% during May). Scatterometer data (here ASCAT) has about the same data density as radiometer during the cold season (from mid-October until end of March), but it is more adequate to infer drift vectors during freeze period with about 50% of the ice-covered area (September-October) and at the beginning of melt onset (April-May). The data density strongly decreases at the end of November 2007 for the ASCAT sensor drift data and in April 2008 for SSM/I sensor drift data. These sharp decreases are directly linked to missing data on the original fields (brightness temperatures for SSM/I and backscatter for ASCAT). Note that when one day original field has low spatial coverage (for example October 29, 2007 with ASCAT), two drift maps are impacted with low data density (at three-day lag, drift map of October 26 until 29 and drift map of October 29 until November 2). One benefit of the merged product is clearly shown in Fig. 3 : the combination of the data increases sharply the data density with more than 80% from

December until mid-May, and 60 to 80% at the beginning of the winter : the merging enables increasing the drift data density by about 20 to 30% at the beginning of the winter and by about 10% during the winter.

In order to have almost full maps, we have developed a space and time interpolation to infer drift in some data gap patches of the sea ice drift merged product at three-day lag (and only for the missing points). For a missing vector, the space interpolation is based on a 9 x 9 pixels area centered on the missing vector. The missing vector is inferred from surrounding vectors if there are enough vectors, as a function of the distance of the surrounding vectors and their "quality" (a vector has the best quality when identical drift has been inferred from the three estimates from SSM/I-H, SSM/I-V and scatterometer data). This has been done from the less isolated missing points to the more isolated points in the map through a loop, in order to fill in most of the missing points. In addition to this space interpolation, a time interpolation is added, based on the drift estimation in the same area for the day before and the day after, with a 70% weight for the studied map and 15% for the day before and day after maps.

Figure 4 shows the steps of the drift estimation at three-day lag in October at the beginning of the winter: drift field from ASCAT scatterometer (Fig. 4a), the merging with radiometer data (Fig. 4b), the interpolation of the missing points (Fig. 4c). This highlights the increase of number of available drift from about 50% for the scatterometer drift field (Fig. 4a) towards the almost full maps with the merged interpolated field (Fig. 4c). In Fig. 3, the interpolated merged product density (in brown) is more than 80% during all the period, with about 5% more than the merged product during November-April period, and about 10% more for the beginning of season (September-October). The merging and the interpolation enable to estimate drift fields during freeze and the beginning of melt period from September until May

with more than 80% drift data density, which is an interesting and sharp improvement of the individual fields for the use of these data.

B. Medium resolution product

Since 2002 and until October 4th 2011, AMSR-E sensor has provided brightness temperature maps at 89 GHz H and V channels with a pixel resolution of 6.25 km, which is interesting to detect small drifts magnitude. From these maps, a merged drift of the two channels is inferred with a 31.25 km grid spacing which we call "medium resolution" in comparison with the low resolution SSM/I/scatterometer drift data presented before. The enhanced resolution also translates in greatly reducing the quantification noise at three and six-day lags, and even enables to compute a two-day lag dataset. Fig. 5 shows the AMSR-E merged drift field at three-day lag for the same period as Fig. 1. Colors show the merging of the two channels. The two maps present similar drift pattern. AMSR-E drift product has a better angular resolution than the low resolution product, but also more data gaps patches and no data around the North Pole. The AMSR-E drift products have been validated with buoys over one winter with standard deviation of 6.2, 6.7 and 8.2 km at two, three and six-day lag respectively, lower than the SSM/I/QuikSCAT results for the same period for the same day lags (see Table 2). The merged medium resolution AMSR-E drifts are in slightly better agreement with buoys than the merged low resolution scatterometer/radiometer drifts but the AMSR-E product has lower density drift, in particular it can not be used for freeze and beginning of the melt period with these channels ([21] has shown that summer drifts can be inferred from the 18 GHz AMSR-E channels). The scatterometer/SSMI merged product has a data density higher than 80% for the period December-mid April and higher than 60% for early fall and early spring,

whereas AMSR-E provides 50 to 80% data density from December to April, and decreases for early fall down to 15 to 60%.

It is tempting to merge drift fields at several resolutions to improve the drift data density and/ or increase the confidence in the field itself. Although the AMSR-E grid resolution is an oversampled of the merged low resolution grid, the merging of these datasets should be handled very carefully because of their different statistical properties. This was not tested here.

IV. Discussion and conclusion

Sea ice drift can be estimated over the whole Arctic area from daily maps of brightness temperature from radiometers and backscatter from scatterometer at low and medium resolutions during the cold season using time lags of two to six days. Due to sensitivity to atmospheric water vapour and ice and snow surface properties, these low and medium resolution microwave high frequency data are not usable in summer to infer sea ice drift since the surface properties change quickly.

This daily coverage of the full Arctic is not possible with buoys data, which offer a better time resolution but a very sparse spatial distribution. Radiometer sea ice drifts are accurate but are limited by the loss of data at the beginning and the end of the cold period. Sea ice drift has been inferred from correlation techniques as demonstration with several sensors, and we show here that combination of satellite sensors drift data enables to have an ongoing long time series with low resolution drift estimation from freeze until the beginning of melt onset.

We have shown that scatterometer drifts are a useful complement to infer a merged drift field at low resolution. Recently, the merging of the two 89 GHz AMSR-E radiometer drift field at medium resolution provides a better angular resolution than the scatterometer/radiometer merged product because of its enhanced ground resolution, which also allows a reduction of the time lag to two days. Both Ku and C-band scatterometers have been used to estimate low resolution sea ice drift. We have shown here that the merging of these drifts with radiometer drifts at the same resolution has several benefits. The objective combination provides more reliable drifts vectors than each individual ones since each drift is inferred from independent measurement and the merging process enables discrimination of the few vector outliers remaining in the individual fields. The combination increases the drift data density, in particular at early fall and early spring with more than 60% data density whereas radiometer-only drift density is 15 to 60% (see Figure 3). Thanks to the combination and a space and time interpolation, 10% more drift vectors can be estimated, enabling to estimate drift at freeze and beginning of melt period. The space and time interpolation of the product enables drift data density to be increased up to 80% to 90% of the maps during the autumn-winter-spring extended season.

In practice, from a useful time frame of October to April using radiometer or scatterometer data alone, the merged product is reliable from September until May. As a result, drift can be inferred during the yearly sea ice minimum extent in September, as shown in Fig. 6 with an example of a three-day lag estimation from 15 until 18 September 2009 with an almost full map presenting a clockwise drift motion. Background colors correspond to the September 15th 2009 ASCAT incidence-adjusted daily averaged backscatter values, this day corresponds to the yearly minimum sea ice extent day when sea ice is multiyear ice. The joint use of drift

field and backscatter data (related to sea ice roughness and thus to ice type) during the following months can provide a continuous view of the multiyear sea ice displacement.

Advantages and shortcomings of each product depend on pixel sizes, period and magnitude of the drift. Noise level is dominated by footprint of the sensor and pixel size. Since the MCC is used, the theoretical absolute and constant uncertainty is related to pixel size. The impact of this uncertainty becomes less important as the drift increases. The optimum day lag must be selected as the expected magnitude of the drifts. The three-day lag product is adapted to estimate high drift magnitude (which is not detected at six-day lag due to de-correlation). The main limitation of the three-day lag low resolution fields is the angular resolution for small drifts. The six-day lag product is suitable for small drift estimation. The selected day lag must be long enough to minimize this impact -but the ability to track the displacements may decreases- and short enough so that features can be identified. This depends upon the ultimate uses of the product.

Since 1992, enhanced merged sea ice drift fields at 62.5 km grid resolution are available at three and six-day lags, first with the combination of the H and V SSM/I channels (1992-1999), then with the SSM/I and the Ku-band QuikSCAT scatterometer data (1999-2009) and since 2007, the time series is ongoing with the C-band ASCAT scatterometer data. The almost full maps at three and six-day lag enable constructing composite monthly eulerian drift maps with almost full maps. This almost 20-years drift data time series is available freely at IFREMER/CERSAT and is updated and continuous by the next C-band ASCAT scatterometers (onboard MetOp-B and -C until 2020) providing a long time series for climate modelling and sea ice studies. The AMSR-E merged drift product at 31.25 km grid resolution is available for the 2002-2011 period (at time of finishing this manuscript, the AMSR-E

sensor stopped recording data on October 4th 2011), the time series will continue with AMSR-E 2 (launch scheduled in 2012).

Thanks to the use of the successive Ku (QuikSCAT) and C-band (ASCAT) scatterometers, a long time series including both datasets is available and ongoing. The main difference we have between the two scatterometers data are the ranging of data over sea ice : the Ku-band data have a wide range of variations, which yields the Ku-band sensor more useful for multi-year ice detection for example; whereas the C-band sensor is less sensitive to surface wetness, including wet snow. For sea ice drift estimation, the C-band data would be more suitable for September data but this benefit is partly blurred by the foot print size of the ASCAT sensor and the scanning geometry yielding a partial daily coverage of the Arctic area. There are thus less drift data density using C-band (ASCAT) data than Ku-band (QuikSCAT) data for the same period. In the near future, the use of both ASCATs on MetOp-A and -B (to be launched in 2012) will greatly increases the daily coverage over polar areas and thus the merged product will further benefit from more C-band data, particularly at the beginning and the end of the winter.

Efforts have been made to combine satellite derived motion with buoys drift [10, 22], which reduced data gaps. Using buoy data is a very nice way of extending sea ice drift maps through the summer and fill this seasonal gap in the annual sea ice motion record. There is a large resolution gap between the satellite products we present and the motion sampled by a buoy. As for the merging of our medium and low resolution products, the merging with buoys motion was not investigated here. It should be noted that using buoys data prevents to have a near real time available time series.

Drift datasets are useful for several applications. Among others, the IFREMER/CERSAT Merged drift datasets presented here are used to study trends in sea ice drift and related processes [23], also to estimate pollution origin using backward trajectory (H. Goodwin from the Norwegian Polar Institute, *personal communication*), and to estimate sea ice flux, for example in Fram Strait [24]. These datasets are also used for sea ice model validation [25, 26]. Recently, ref. [27] has compared the satellite drifts with the ocean-sea ice coupled North Atlantic-Arctic Ocean-Sea-Ice Model modelled drifts in the Laptev shelf sea. Preliminary effort has been done comparing drift datasets at several resolutions and with different methods in the Laptev sea. They show that the satellite inferred drifts present good estimate in this shelf region, in particular the merged medium-resolution AMSR-E drifts product with the robust MCC technique presented here has a high correlation and low standard deviation compared with the buoys data.

Drift datasets are also used to improve sea ice model at large scale, complementary to sea ice concentration, for example through data assimilation [28]. Assimilation of motion is particularly suited for improving the simulation of specific synoptic events [29]. Ref [30] uses SSM/I sea ice motion dataset for assimilation, this improves ice outflow in Fram Strait, enhances ice deformation computed by the model, and increases the correlation between observations and model. Assimilation of the merged low resolution product presented here has been tested by the UK MetOffice in the Forecasting Ocean Atmospheric Model: with the assimilation of the three-day lag field, the drift pattern becomes closer to the observed drift [31]. Ref. [32] has also shown that assimilation of these fields greatly improves results on the modelled drift but also on sea ice concentration and thickness. Assimilation of the medium resolution AMSR-E products presented here in the operational Towards an Operational Prediction system for the north Atlantic European coastal Zones system enables the modelled

sea ice thickness to be more reliable [33], this improvement has been also noted with assimilating other drift datasets [29, 30].

The new interpolated merged field has the advantage to be gap-filled motion fields ready-to-use in models, and to have an expanded autumn-winter-spring season (from September until May) which is useful for all these applications.

Acknowledgement

Daily backscatter and drift data are available at IFREMER/CERSAT (http://cersat.ifremer.fr). The authors thank the CERSAT team, in particular Denis Croizé-Fillon, for acquisition and archiving of the satellite data and the systematic processing of the sea ice drift maps. We thank also Julien Paul for the space and time interpolation tool development. We are grateful also to the reviewers for their helpful comments which improved the manuscript, and to F. Ardhuin for English reviews. SSM/I data are provided by National Snow and Ice Data Center, University of Colorado (USA), AMSR-E data by University of Bremen (Germany), QuikSCAT L2A data by Physical Oceanographic Data Active Archiving Center (PODAAC)/Jet Propulsion Laboratory (USA), and ASCAT L1 data by EUMETSAT. The International Arctic Buoy Programme buoys data are provided by the Polar Science Center, University of Washington (USA). This study was partly supported by the DAMOCLES project, financed by the European Union in the 6th framework program for research and development, and the Centre National d'Etudes Spatiales. The Global Monitoring for Environment and Security European Union projects PolarView and MyOcean support partly the data production and distribution.

References

[1] K. Aagaard, J. H. Swift, and E. C. Carmack, "Thermohaline circulation in the Arctic Mediterranean seas", *J. Geophys. Res.*, *vol. 90* (C3), pp. 4833-4846, 1985.

[2] R. Colony, and S. Thorndike, "An estimate of the mean field of Arctic sea ice motion", *J. Geophys. Res.*, *vol. 89* (C6), pp. 10623-10629, 1984.

[3] W.J. Emery, C. W. Fowler, J. Hawkins, and R. H. Preller, "Fram strait satellite image-derived ice motions", *J. Geophys. Res.*, *vol. 96* (C3), pp. 4751-4768, 1991.

[4] J. Haarpaintner, "Arctic-wide operational sea ice drift from enhanced-resolution QuikSCAT/SeaWinds scatterometry and its validation", *IEEE Trans. Geosci. Remote. Sens., vol. 44* (1), doi :10.1109/TGRS.2005.859352, 2006.

[5] R. Kwok, J.C. Curlander, R. McConnell, and S. S. Pang, "An ice motion tracking system at the Alaska SAR Facility", *IEEE J. Oceanic Eng.*, *vol. 15* (1), pp. 44-54, 1990.

[6] C.A. Geiger and M.R. Drinkwater, "Coincident buoys -and SAR-derived surface fluxes in the western Weddel sea during ice station Weddell 1992", *J. Geophys. Res.*, *vol. 110* (C04002), doi:10.1029/2003JC002112, 2005.

[7] F. Gohin and A. Cavanié, "A first try at identification of sea ice using the three beam scatterometer ERS-1', *Int. J. Remote Sensing*, *vol. 15* (6), pp. 1221-1228, 1994.

[8] R. Kwok, A. Schweiger, D. A. Rothrock, S. Pang, and C. Kottmeier, “Sea ice motion from satellite passive microwave imagery assessed with ERS SAR and buoy motions”, *J. Geophys. Res.*, *vol. 103* (C4), pp. 8191-8214, 1998.

[9] T. Martin and E. Augstein, “Large-scale drift of Arctic sea ice retrieved from passive microwave satellite data”, *J. Geophys. Res.*, *vol. 105* (C4), pp. 8775-8788, 2000.

[10] A.K. Liu, Y. Zhao, and S. Y. Wu, “Arctic sea ice drift from wavelet analysis of NSCAT and special sensor microwave imager data”, *J. Geophys. Res.*, *vol. 104* (C5), pp. 11529-11538, 1999.

[11] R.G. Onstott and S.P. Gogineni, “Active microwave measurements of Arctic sea ice under summer conditions”, *J. Geophys. Res.*, *vol. 90* (C3), pp. 5035-5044, 1985.

[12] W.J. Emery, C. W. Fowler, and J. A. Maslanik, “Satellite-derived maps of Arctic and Antarctic sea ice motion: 1988 to 1994”, *Geophys. Res. Lett.*, *vol. 24* (8), pp. 897-900, 1997.

[13] R.M. Ninnis, W. J. Emery, and M. J. Collins, “Automated extraction of pack ice motion from Advanced Very High Resolution Radiometer imagery”, *J. Geophys. Res.*, *vol. 91* (C9), pp. 10725-10734, 1986.

[14] M. Kamachi, “Advective surface velocities derived from sequential images for rotational flow field : limitations and applications of Maximum Cross Correlation method with rotational registration”, *J. Geophys. Res.*, *vol. 94* (C12), pp. 18227-18233, 1989.

[15] T. Lavergne, S. Eastwood, Z. Teffah, H. Schyberg, and L.A. Breivik, “Sea ice motion from low-resolution satellite sensors: an alternative method and its validation in the Arctic”, *J. Geophys. Res.*, *vol. 115* (C10032), doi :10.1029/2009JC005958, 2010.

[16] L. Kaleschke, C. Lüpkes, T. Vihma, J. Haarpaintner, A. Bochert, J. Hartmann, and G. Hegster, "SSM/I sea ice remote sensing for mesoscale ocean-atmosphere interaction analysis", *Canadian Journal of Remote. Sens., vol. 27* (5), 2001, pp 526-537.

[17] A.K. Liu and D. J. Cavalieri, "On sea ice drift from the wavelet analysis of the Defense Meteorological Satellite Program (DMSP) Special Sensor Microwave Imager (SSM/I) data", *Int. J. Rem. Sens.*, *vol. 19* (7), pp. 1415-1423, 1998.

[18] A.S. Thorndike. and R. Colony, "Sea ice motion in response to geostrophic winds", *J. Geophys. Res.*, *vol. 87,* pp. 5845-5852, 1982.

[19] R. Ezraty, and A. Cavanié, "Construction and evaluation of 12.5-km grid NSCAT backscatter maps over sea ice", *IEEE Trans. Geosci. Remote. Sens., vol. 37* (3), 1999, pp 1685-1697.

[20] Y. Zhao, A. K. Liu, and D. G. Long, "Validation of sea ice motion from QuikSCAT with those from SSM/I and buoy", *IEEE Trans. Geosci. Remote. Sens., vol. 40* (6), pp. 1241-1246, 2002.

[21] R. Kwok, "Summer sea ice motion from the 18 GHz channel of AMSR-E and the exchange of sea ice between the Pacific and the Atlantic sectors", *Geophys. Res. Lett.*, *vol. 35* (L03504), doi:10.1029/2007GL032692, 2008.

[22] C.W. Fowler, 2003 (updated 2008); *Polar Pathfinder Daily 25 km EASE grid sea ice motion vectors. Boulder, Colorado, USA : National Snow and Ice Data Center.*

[23] G. Spreen, R. Kwok, and D. Menemenlis, “Trends in Arctic sea ice drift and role of wind forcing:1992-2009”, *Geophys. Res. Lett.*, *vol. 38* (L19501), doi:10.1029/2011GL048970, 2011.

[24] G. Spreen, S. Kern, D. Stammer, and E. Hansen, “Fram strait sea ice volume export estimated between 2003 and 2008 from satellite data”, *Geophys. Res. Lett.*, *vol. 36* (L19502), doi:10.1029/2009GL039591, 2009.

[25] T. Martin and R. Gerdes, “Sea ice drift variability in Arctic ocean model intercomparison project models and observations”, *J. Geophys. Res.*, *vol. 112* (C04S10), doi:10.1029/2006JC003617, 2007.

[26] F. Girard-Ardhuin, D. Croizé-Fillon, G. Garric, and C.-E. Testut, “Improving models with global scale sea ice data from satellites”. *IAMAS-IAPSO, IACS Joint assembly MOCA-09, Montréal, Canada. 19-29 July 2009.*

[27] P. Rozman, J. Hölemann, T. Krumpen, R. Gerdes, C. Köberle, T. Lavergne, S. Adams, and F. Girard-Ardhuin, “Validating satellite derived and modeled sea ice drift in the Laptev sea with In Situ measurements of winter 2007/08”. *Polar Research 2011, 30*, 7218, doi: 10.3402/polar.v30i0.7218.

[28] V. Dulière and T. Fichefet, “On the assimilation of ice velocity and concentration data into large-scale sea ice models”. *Ocean Sci., vol. 3*, pp. 321-335, 2007.

[29] W.N. Meier, J. A. Maslanik, and C. W. Fowler, “Error analysis and assimilation of remotely sensed ice motion within an Arctic sea ice model”, *J. Geophys. Res.*, *vol. 105* (C2), pp. 3339-3356. 2000.

[30] J. Zhang, D. R. Thomas, D. A. Rothrock, R. W. Lindsay, Y. Yu, and R. Kwok, "Assimilation of ice motion observations and comparisons with submarine ice thickness data", *J. Geophys. Res.*, *vol. 108* (C6), doi:10.1029/2001JC001041, 2003.

[31] J. Stark, J. Ridley, M. Martin, and A. Hines, "Sea ice concentration and motion assimilation in a sea ice-ocean model", *J. Geophys. Res.*, *vol. 113* (C05S91), doi :10.1029/2007JC004224, 2008.

[32] K. Rollenhagen, R. Timmermann, T. Janjic, J. Schröter, and S. Danilov, "Assimilation of sea ice motion in a finite-element sea ice model". *J. Geophys. Res.*, *vol. 114* (C05007), doi:10.1029/2008JC005067, 2009.

[33] L. Bertino, P. Sakov, and F. Counillon, "The TOPAZ sea ice and ocean pilot reanalysis (2003-2008)". *European Geophysical Union General Assembly meeting, 3-8 April 2011, Vienna, Austria*. 2011.

Fanny Girard-Ardhuin (M'03) received her Ph. D. in radar meteorology at the Laboratoire d'Aérologie (Toulouse, France) in 2001. Her thesis deals with atmospheric boundary layer studies, using wind profiler radar with Radio Acoustic Sounding System (RASS). Research fellow at Telecom Bretagne (Brest, France) in 2002, she analyzed Synthetic Aperture Radar data, in particular for oil spill detection. She joined what is now Division of Radar Application of Collecte Localisation Satellites in 2003 to implement oil slick detection algorithms and test synergistic data analysis for slick classification. Since 2004 at the Institut Français de Recherche pour l'Exploitation de la Mer (IFREMER, Brest, France), she is involved in sea ice monitoring from active and passive sensors, in particular for sea ice drift estimation and multi-year ice detection. She is currently a member of the ESA/ASCAT-MetOp Science Advisory Group.

Robert Ezraty holds an engineer degree from Ecole d'Ingénieur de Marseille (France) in 1968 and received the Dr-Ing. Degree in fluid mechanics from the Institut de Mécanique Statistique de la Turbulence (Marseille, France) in 1971. He joined what is now Institut Français de Recherche pour l'Exploitation de la Mer (IFREMER, Brest, France) in 1974. He has studied surface waves and winds at sea and has been in charge of a calibration/validation program for ESA's ERS-1 altimeter and scatterometer. Since 1992, he has been involved in sea ice studies at polar ocean scales using both active and passive sensors from various satellite missions.

Figures captions

Figure 1 : Arctic sea ice drift map from independent maps of drift vector from : SSM/I H and SSM/I V polarization channels, and SeaWinds/QuikSCAT. The time lag is three days: April 24-27, 2007. Drift vectors less than one pixel are marked by a cross. Identical drift vectors for the three estimates is colored in red; identical drift vectors for any two of the estimates is colored in green; selection or validation of any single drift vector is colored in blue. Note that the arrows are not at the scale of the map.

Figure 2 : Angle difference between satellite merged drift vectors and buoys drift vectors as a function of the merged drift magnitude. The time lag is three days. The comparison spans over five winters. Colors represent the percentage of occurrence expressed in logarithm scale.

Figure 3 : Times series of the density of drift vectors during the 2007-2008 winter. The time lag is three days. Green and blue represent respectively the SSM/I H and V polarization data, black is ASCAT, red is the merged SSM/I/ASCAT data and brown is the filled product.

Figure 4 : Arctic sea ice drift maps for October 3-6, 2007 (three-day lag). a) ASCAT estimates, b) merged ASCAT/SSM/I H and V polarizations channels drift estimates, c) space and time interpolation applied to the b). Drift vectors less than one pixel are marked by a cross. Note that the arrows are not at the scale of the map.

Figure 5 : Arctic sea ice drift map from the combination of 89 GHz AMSR-E channels (H and V polarizations) for April 24-27, 2007. The time lag is three days. Drift vectors less than one pixel are marked by a cross. In red : identical drift vectors for the two fields, in blue :

selection or validation of any single vector. Note that the arrows are not at the scale of the map.

Figure 6 : Arctic sea ice merged ASCAT/SSM/I drift fields for September 15-18, 2009. The time lag is three days. Drift vectors less than one pixel are marked by a cross. Note that the arrows are not at the scale of the map. Background colors represent ASCAT incidence-adjusted daily averaged backscatter values on September 15th, 2009.

rms drift difference (cm s^{-1})	rms direction difference (°)	day lag (nb of days)	sensor	reference
6		**1**	**SSM/I**	**[12]**
2.6[#]	**25.9[#]**	**1**	**SSM/I**	**[17]**
2.9[##]	**18.0[##]**	**1**	**SSM/I**	
11.1	**46.5**	**3**	**SSM/I V**	
6.7[e]	**30.6[e]**	**3**	**SSM/I V**	**[8]**
11.7	**50.4**	**3**	**SSM/I H**	
7.5[e]	**32.8[e]**	**3**	**SSM/I H**	
3.3* and 3.1[#]	**37.8* and 29.4[#]**	**4**	**SSM/I**	**[10]**
2.8* and 2.0[#]	**32.4* and 17.1[#]**	**4**	**NSCAT**	
2.27[e]	**35.5[e]**	**4**	**SSM/I**	**[20]**
2.32[e]	**29.8[e]**	**4**	**QuikSCAT**	

Table 1

Some results of the comparisons between satellite drift vectors and buoys drifts for several experiments: standard deviation for sea ice drift magnitude difference and for direction difference, number of day lag, satellite sensor, and reference. *result for November, [#] results for December, [##] results for January, [e] excluding small drifts (less than one pixel).

rms drift magnitude difference (km)	rms drift difference (cm s^{-1})	rms direction difference (°)	day lag (nb of days)	product	period
7.5	**2.91**	**39.2**	**3**	**Merged SSM/I & QuikSCAT**	**five winters**
7.5[e]	**2.90[e]**	**29.6[e]**	**3**		
8.9	**1.72**	**29.6**	**6**		
9.1[e]	**1.76[e]**	**24.3[e]**	**6**		
8.1	**3.14**	**35.1**	**3**	**Merged SSM/I & QuikSCAT**	**one winter**
10.8	**2.08**	**27.0**	**6**		
6.2	**3.61**	**39.9**	**2**	**Merged AMSR-E H & AMSR-E V**	
6.7	**2.60**	**35.2**	**3**		
8.2	**1.59**	**26.8**	**6**		

Table 2

Results of the comparisons between satellite drift vectors (merged drifts at low and medium resolution) and buoys drifts: standard deviation for sea ice drift difference (magnitude and velocity) and for direction difference, number of day lag, product and period. [e] excluding small drifts (less than one pixel).

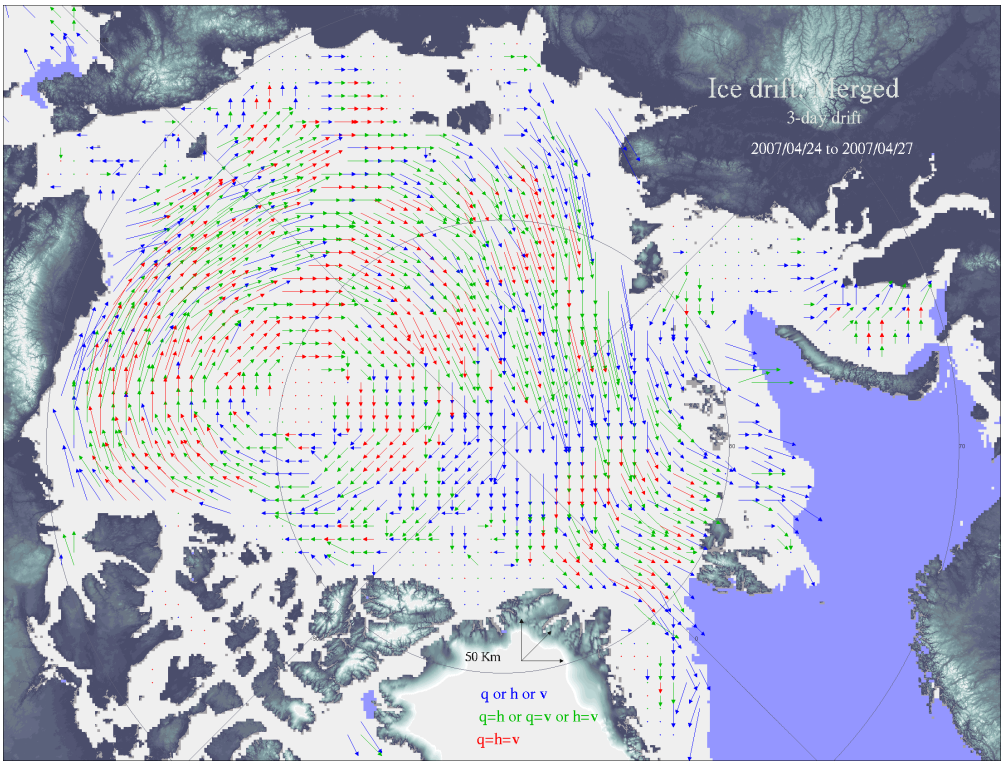
Ice drift: Merged
3-day drift
2007/04/24 to 2007/04/27
50 Km
q or h or v
q=h or q=v or h=v
q=h=v

Fig 1

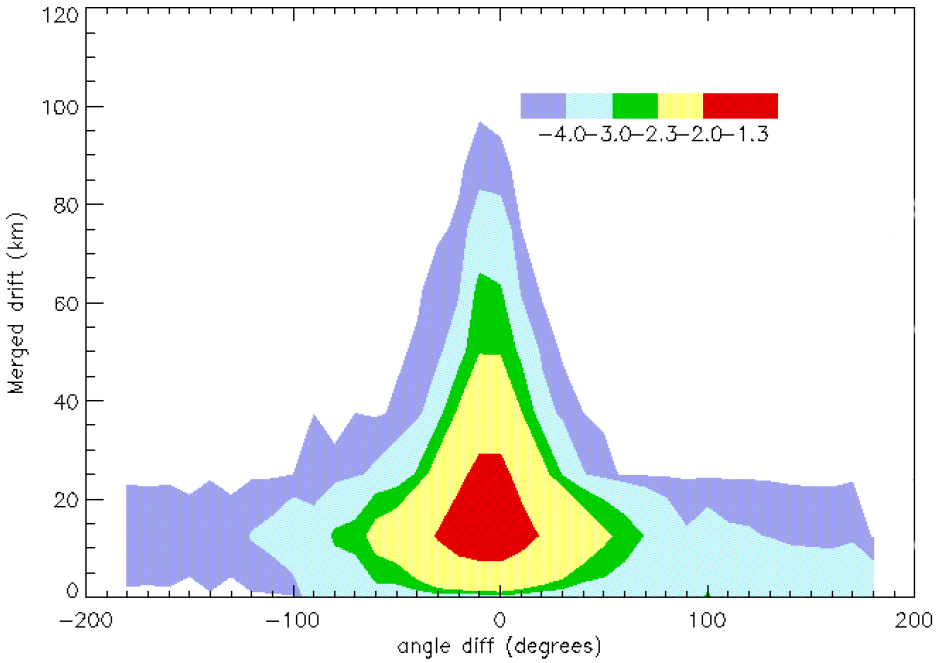
120
100
80
60
40
20
0
Merged drift (km)
−4.0−3.0−2.3−2.0−1.3
−200
−100
0
100
200
angle diff (degrees)

Fig 2

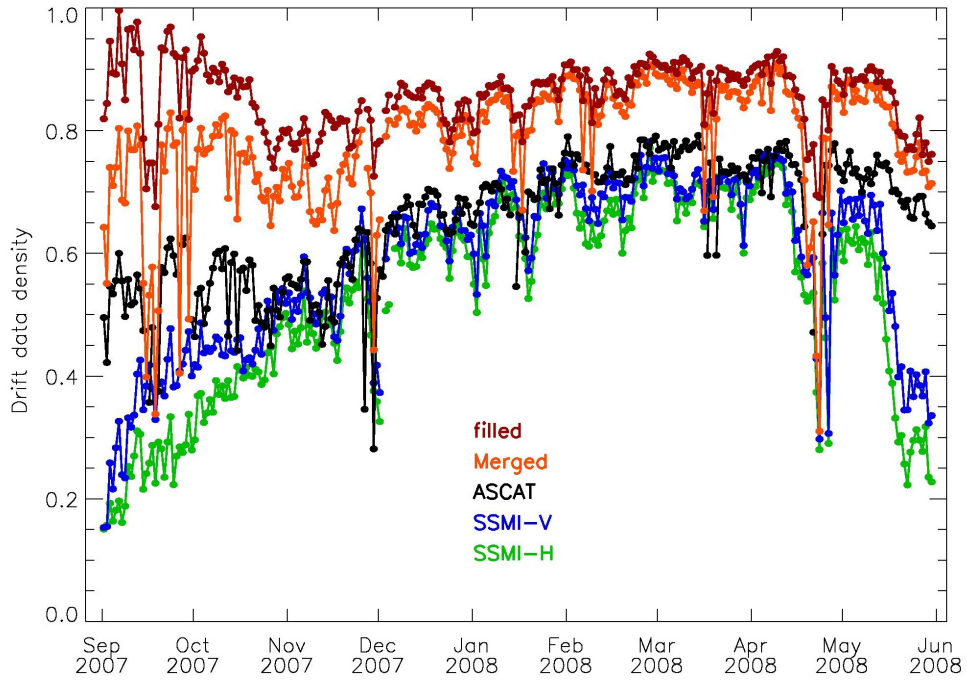
Drift data density
1.0
0.8
0.6
0.4
0.2
0.0
Sep 2007
Oct 2007
Nov 2007
Dec 2007
Jan 2008
Feb 2008
Mar 2008
Apr 2008
May 2008
Jun 2008
filled
Merged
ASCAT
SSMI–V
SSMI–H

Fig 3

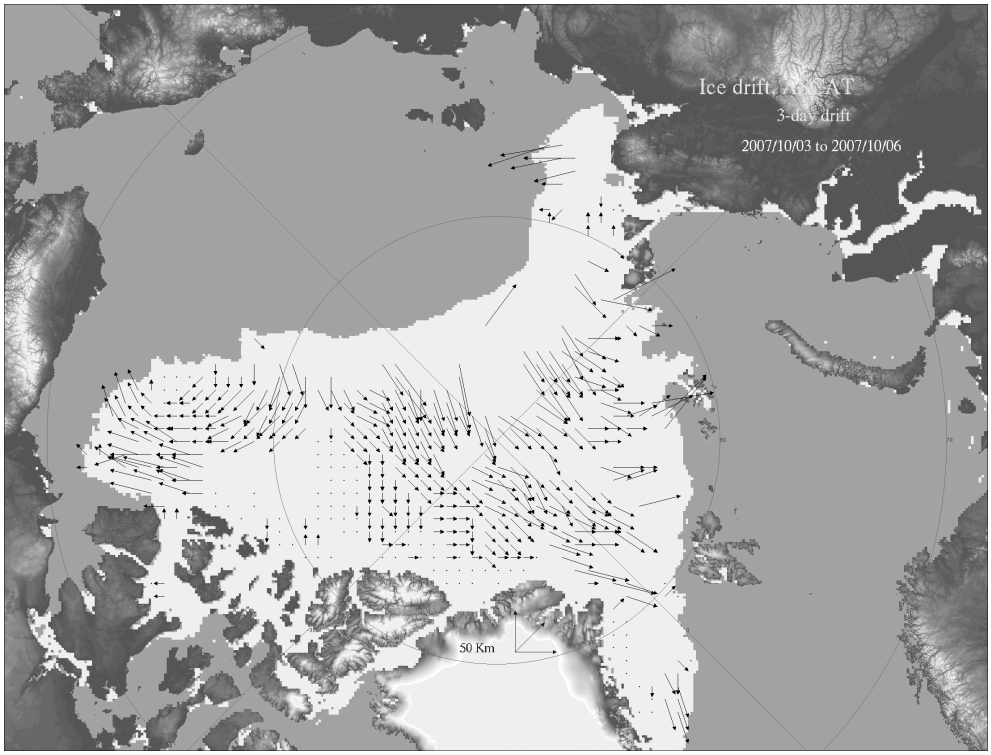
Ice drift, ASCAT
3-day drift
2007/10/03 to 2007/10/06
50 Km

Fig. 4a

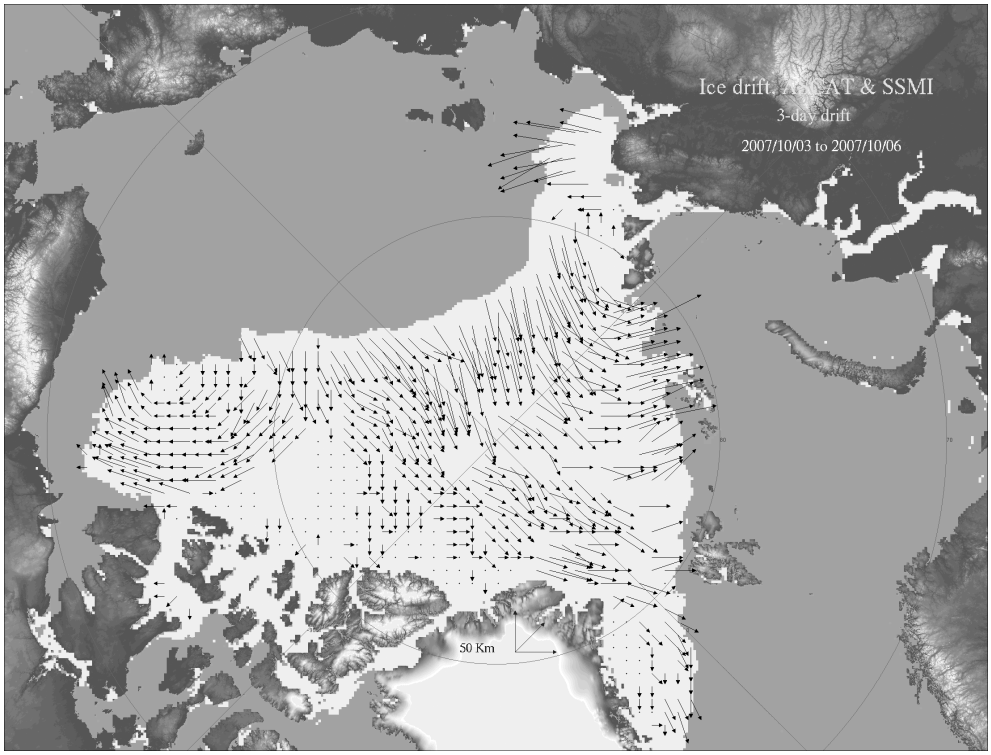
Ice drift, AVHRR, AT & SSMI
3-day drift
2007/10/03 to 2007/10/06
50 Km

Fig 4b

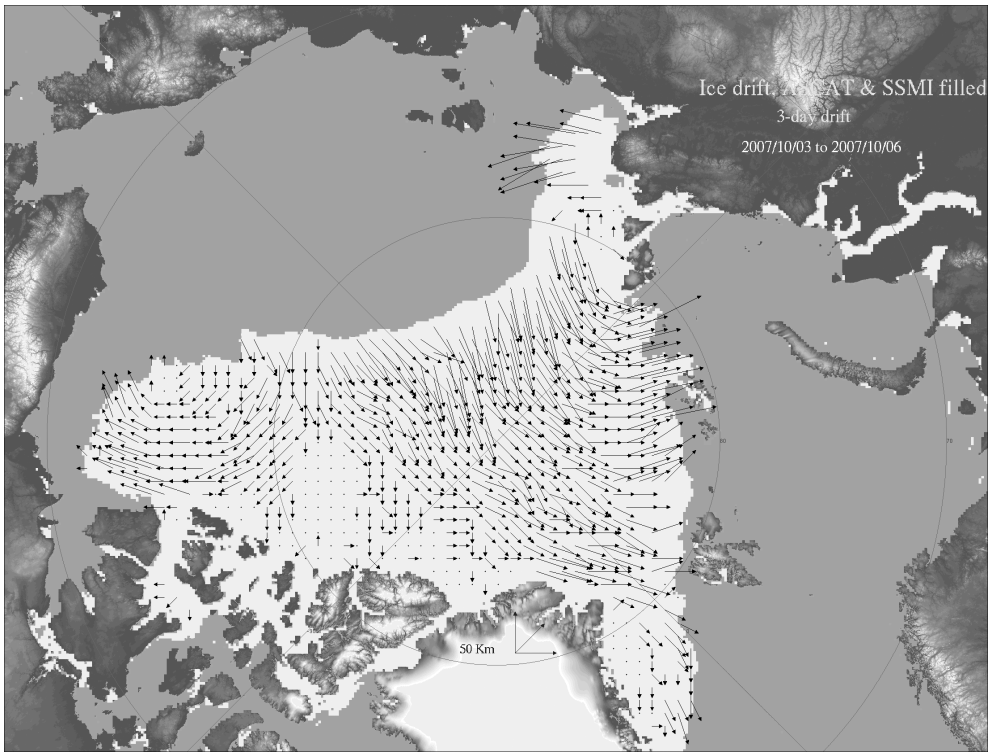
Ice drift, AVHRR, AT & SSMI filled
3-day drift
2007/10/03 to 2007/10/06
50 Km

Fig. 4c

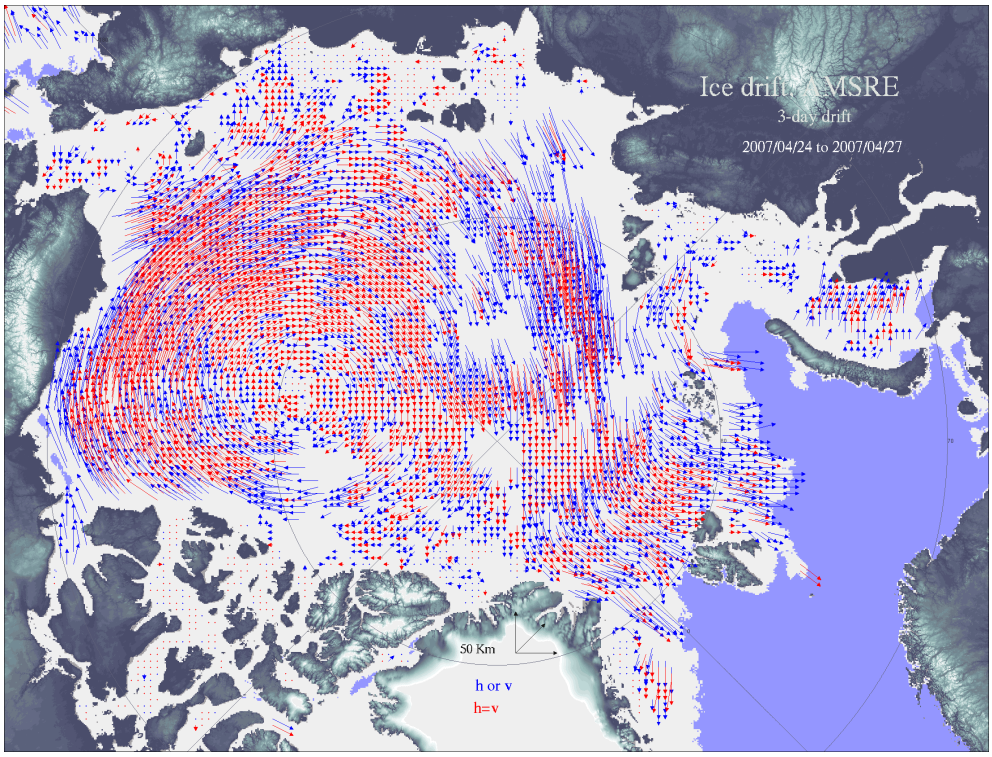
3-day drift
2007/04/24 to 2007/04/27
50 Km
h or v
h=v

Fig 5

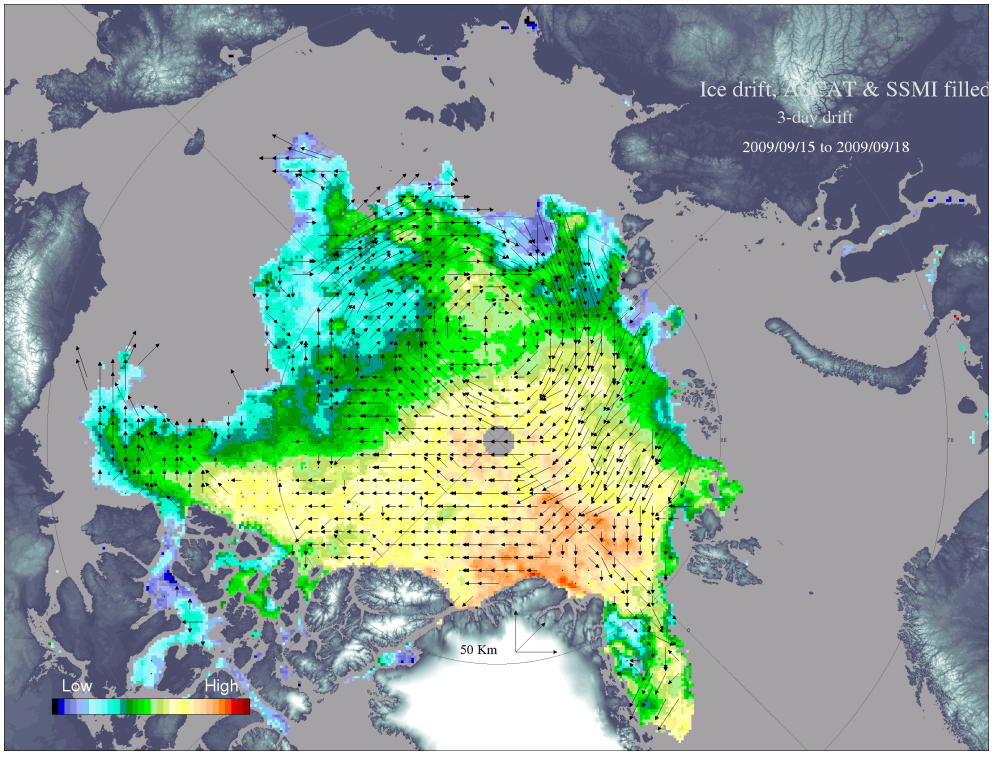
3-day drift
2009/09/15 to 2009/09/18
50 Km
Low
High

Fig 6